Reproducibility of image quality for moving objects using respiratory-gated computed tomography: A study using a phantom model

Article *in* Journal of Radiation Research · September 2012

DOI: 10.1093/jrr/rrs039 · Source: PubMed

CITATIONS
11

READS
239

10 authors, including:

Toshiyuki Terunuma
University of Tsukuba
64 PUBLICATIONS **978** CITATIONS
SEE PROFILE

Masashi Mizumoto
St. Jude Children's Research Hospital
205 PUBLICATIONS **3,270** CITATIONS
SEE PROFILE

Takashi Moritake
University of Occupational and Environmental Health
69 PUBLICATIONS **1,395** CITATIONS
SEE PROFILE

Toshiyuki Okumura
University of Tsukuba
200 PUBLICATIONS **3,094** CITATIONS
SEE PROFILE

Journal of Radiation Research, 2012, 53, 945–953
doi: 10.1093/jrr/rrs039 Advance Access Publication 10 September 2012

Reproducibility of image quality for moving objects using respiratory-gated computed tomography: a study using a phantom model

Nobuyoshi FUKUMITSU[1,2,*], Masaya ISHIDA[1], Toshiyuki TERUNUMA[1], Masashi MIZUMOTO[1], Takayuki HASHIMOTO[1], Takashi MORITAKE[1], Toshiyuki OKUMURA[1], Takeji SAKAE[1], Koji TSUBOI[1] and Hideyuki SAKURAI[1]

[1]Proton Medical Research Center, University of Tsukuba, Tsukuba, Japan
[2]Department of Radiation Oncology, Ibaraki Prefectural Central Hospital, Ibaraki, Japan
*Corresponding author. Department of Radiation Oncology, Ibaraki Prefectural Central Hospital, 6528, Koibuchi, Kasama, Ibaraki, 309-1793, Japan; Tel: 81-29-677-1121; Fax: 81-29-677-2886; Email: fukumitsun@yahoo.co.jp

(Received 29 February 2012; revised 22 April 2012; accepted 28 May 2012)

To investigate the reproducibility of computed tomography (CT) imaging quality in respiratory-gated radiation treatment planning is essential in radiotherapy of movable tumors. Seven series of regular and six series of irregular respiratory motions were performed using a thorax dynamic phantom. For the regular respiratory motions, the respiratory cycle was changed from 2.5 to 4 s and the amplitude was changed from 4 to 10 mm. For the irregular respiratory motions, a cycle of 2.5 to 4 or an amplitude of 4 to 10 mm was added to the base data (i.e. 3.5-s cycle, 6-mm amplitude) every three cycles. Images of the object were acquired six times using respiratory-gated data acquisition. The volume of the object was calculated and the reproducibility of the volume was decided based on the variety. The registered image of the object was added and the reproducibility of the shape was decided based on the degree of overlap of objects. The variety in the volumes and shapes differed significantly as the respiratory cycle changed according to regular respiratory motions. In irregular respiratory motion, shape reproducibility was further inferior, and the percentage of overlap among the six images was 35.26% in the 2.5- and 3.5-s cycle mixed group. Amplitude changes did not produce significant differences in the variety of the volumes and shapes. Respiratory cycle changes reduced the reproducibility of the image quality in respiratory-gated CT.

Keywords: Respiratory-gated CT; thorax phantom; respiratory motion; lung cancer

INTRODUCTION

Computed tomography (CT) is a standard technology in modern radiation treatment planning. Radiation oncologists recognize tumors as clusters of low- or high-density areas on CT images, indicating the gross tumor volume. However, CT imaging always has some degree of artifact, and this factor can deteriorate the image quality and reduce the reproducibility of the images. In particular, moving tumors in the chest and abdomen can produce serious motion artifacts. Motion artifacts can cause the tumor to appear shortened, elongated or split into several pieces in the cranial–caudal direction [1–3]. Treatment planning based on incorrect and uncertain estimates of the tumor size and shape may lead to improper dose delivery to the tumor and adjacent normal structures.

Respiratory-gated data acquisition was applied to radiotherapy in the 1980s [4]. Respiratory-gated techniques use external respiratory signals on the body surface to calculate and simulate the tumor position in a non-invasive manner and are widely used. The reproducibility of the location has been investigated by numerous researchers by analyzing the reference points or trajectory [5–10]. However, the reproducibility of the image quality of moving tumors using respiratory-gated data acquisition has seldom been investigated.

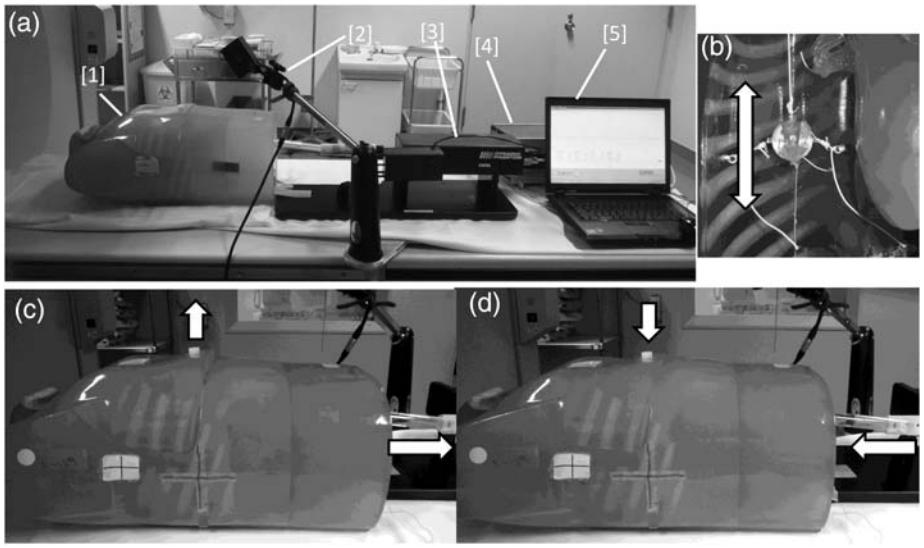

Fig. 1. Respiratory-gated moving phantom system. (**a**) System appearance; [1] chest phantom; [2] laser displacement sensor; [3] actuator; [4] controller; [5] personal computer. (**b**) Sphere object in the right lung field. The diameter is 30 mm, and a small metallic marker is positioned at the center. The sphere moves in a cranial–caudal direction as the rod of the actuator moves. (**c**) Inhalation phase. The anterior chest wall moves upward and the rod of the actuator moves caudally. (**d**) Exhalation phase. The anterior chest wall moves downward and the rod of the actuator moves cranially. The arrows show the direction of movement.

We used a respiratory-gated moving phantom and investigated the reproducibility of CT image quality using regular and irregular patterns of respiratory rhythm.

MATERIALS AND METHODS

A three-dimensional chest phantom was used, as shown in Fig. 1. An acrylic spherical object (30 mm in diameter) was positioned inside the 'right lung field'. This object had a small penetrating hole and a metallic marker (diameter 0.5 mm, length 3 mm) located at the center. This object was then tied in place using four elastic strings toward the upper, medial, lateral and posterior directions and one non-elastic string toward the lower direction. The non-elastic string penetrated outside through the 'diaphragm'. The chest phantom was originally modified to connect with the actuator of the dynamic thorax phantom (model 008A; Computerized Imaging Reference System (CIRS), Inc., Norfolk, VA, USA) [11] so as to produce realistic human respiratory motions. As a piston rod moves in the caudal direction, the anterior chest wall moves upward and the object in the right lung field moves in the caudal direction, similar to the motion during the inhalation phase; then, as the piston rod moves in a cranial direction, the anterior chest wall moves downward and the object moves cranially, similar to the motion during the exhalation phase. The dynamic thorax phantom can be operated using the CIRS motion control software system, and the optional respiratory motion data can be imported using the csv file. We imported several kinds of novel respiratory motion data and obtained CT images of the object to investigate the reproducibility of the image quality.

Regular respiratory rhythms

Seven series of regular respiratory motion data sets were prepared (Table 1). The data for R3 (amplitude: 6 mm, cycle: 3.5 s, form: $\cos^4\theta$) were used as a baseline because the respiratory waveform obtained from the chest wall movement was similar to that of the patients. The amplitude was varied from 4 to 10 mm at 2-mm intervals, and the cycle was varied from 2.5 to 4 s at 0.5-s intervals (Fig. 2).

Irregular respiratory rhythms

Six series of irregular respiratory motion data sets were prepared (Table 1). The irregular respiratory cycles were modified using the data for R3 as the baseline regular respiratory rhythm. Basically, a cycle from 2.5 to 4 s at 0.5-s intervals with the same amplitude and form was inserted into the R3 data every three cycles to create cycle irregularity. The unmodified R3 data were substituted for the insertion of a 3.5-se cycle. An amplitude from 4 to 10 mm at 2-mm intervals with the same cycle and form was inserted into the R3 data every three cycles to create amplitude irregularity. The unmodified R3 data were substituted for the insertion of a 6-mm amplitude (Fig. 2). The scan was performed for 8 cm (16 slices), the number of slices for regular and irregular rhythm was 12 and 4, respectively.

Table 1. Respiratory motion data

	Regular rythm				Irregular rythm		
	cycle (sec)	**amplitude (mm)**	**form**		**cycle (sec)**	**amplitude (mm)**	**form**
R1	2.5	6	$\cos^4\theta$	IR1	3.5 + 2.5	6	$\cos^4\theta$
R2	3	6	$\cos^4\theta$	IR2	3.5 + 3	6	$\cos^4\theta$
R3	3.5	6	$\cos^4\theta$	IR3	3.5 + 4	6	$\cos^4\theta$
R4	4	6	$\cos^4\theta$	IR4	3.5	6 + 4	$\cos^4\theta$
R5	3.5	4	$\cos^4\theta$	IR5	3.5	6 + 8	$\cos^4\theta$
R6	3.5	8	$\cos^4\theta$	IR6	3.5	6 + 10	$\cos^4\theta$
R7	3.5	10	$\cos^4\theta$				

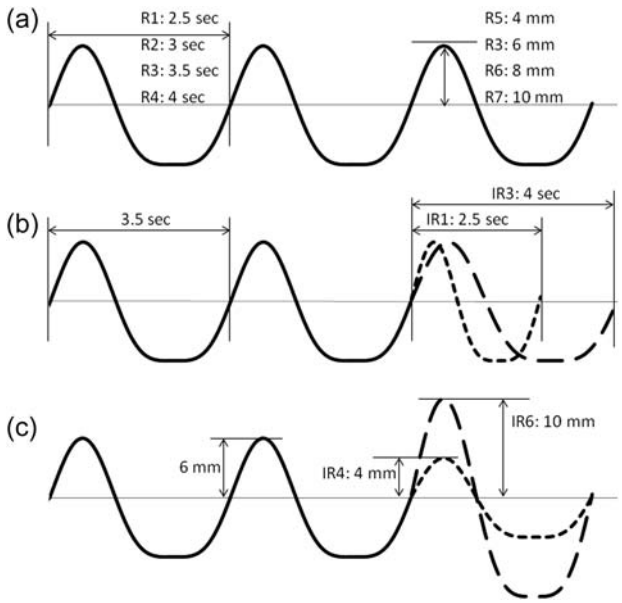

Fig. 2. Regular and irregular motion data. (**a**) Regular respiratory motion data. The amplitude was varied from 4 to 10 mm at 2-mm intervals, and the cycle was varied from 2.5 to 4 s at 0.5-sec intervals on the $\cos^4\theta$ curve. (**b**) Irregular respiratory motion data (cycle). A cycle from 2.5 to 4 s at 0.5-sec intervals with the same amplitude and form was inserted into the R3 data (amplitude: 6 mm, cycle: 3.5 s, form: $\cos^4\theta$) every three cycles. This image shows IR1 (2.5 s) and IR3 (4 s). IR2 (3 s) and R3 (3.5 s, regular) are in between. (**c**) Irregular respiratory motion data (amplitude). An amplitude from 4 to 10 mm at 2-mm intervals with the same cycle and form was inserted into the R3 data (amplitude: 6 mm, cycle: 3.5 s, form: $\cos^4\theta$) every three cycles. This image shows IR4 (4 mm) and IR6 (10 mm). R3 (6 mm, regular) and IR5 (8 mm) are in between.

The CT imaging studies were performed using a CT scanner (W3000AD; Hitachi Medical Corporation, Tokyo, Japan) and the same protocol was adopted as that used for clinical practice at the Proton Medical Research Center, University of Tsukuba, Japan [12–14]. The CT scans were acquired using respiratory-gated acquisition. The respiratory waveform was obtained using a laser displacement sensor that was focused on an area near the phantom's anterior chest wall (5–10 cm in radius). A gate signal was given to enable the exposure when the respiratory waveform dropped below a certain threshold (25% from the peak exhalation on the amplitude scale). The start of exposure was triggered by the gate signal, and the beam was exposed for 1 s. To achieve this exposure, the CT table was moved to the next slice position after scanning. All the slices were scanned using a 5-mm thickness in a direction downwards to the top of the diaphragm. The pitch was 5-mm. The following CT scanning parameters were used: 120 kV, 250 mAs, a field of view of 509×509 mm, and a 512×512 matrix. Images were continuously acquired using three different scanning start positions for a total of six times for each respiratory motion data group. Moreover, a static image was obtained in the same manner and used as a reference.

Image analysis

The image analysis for volume and shape reproducibility was performed using the Dr. View/LINUX software system for image analysis (AJS Inc., Tokyo, Japan).

Volume reproducibility

First, we extracted the slice around the object (approximately 6–7 cm width) and deleted the chest wall and mediastinum manually, thus a CT image of the object was obtained. Next, the object was contoured using an auto-segmentation method and a threshold value (160 Hounsfield units (HU), the most appropriate value for this system). Then, the extracted area was clustered three-dimensionally and the volume was calculated.

Shape reproducibility

First, image registration of the object was performed using one of the CT images as a reference in each group. For

image registration, we used a three-dimensional rigid registration developed by Maes *et al.* [15], the principle algorithm is to shift one image to the position where the overlapping volume of the two objects yields the maximum value. The other five images were registered with the reference image along the three horizontal and three rotational axes. We checked that the images were correctly registered by examining the location of the metallic marker, and supplementary adjustments were performed using the marker as a matching point for some of the images. In this process, the dislocation of the two objects becomes irrelevant to the overlapping volume and can be ignored the analysis. The five images were then re-sliced after image registration. Second, a bitmap image of the object was completed after contouring and clustering in the same manner as mentioned above. Next, an image of the object was constructed by subtracting the outside of the bitmap of the object from the original CT data. During this process, the HU of the object was transformed to a constant value (50 HU). Then, all six images were added. In the added image, the area was divided into seven levels of HU for every 50 HU; 300 HU means that the six objects overlapped, whereas 50 HU means that only one of the objects existed without any overlap and 0 HU means that no objects were present. Finally, we calculated the volume of each HU as an alternate parameter for shape reproducibility (Fig. 3).

Statistical analysis

The value was expressed using the mean value and the standard deviation. Volume reproducibility was examined using a Bartlett test for a multi-group analysis of variance. Shape reproducibility was examined using the chi-squared test. A P value <0.05 was considered significant.

RESULTS

Regular respiratory rhythm study

Cycle changes: R1 (2.5 s), R2 (3 s), R3 (3.5 s) and R4 (4 s).

The volume of the object was 14.03–14.9 (14.49 ± 0.34) cm^3 in the R1 group, 14.29–14.71 (14.44 ± 0.16) cm^3 in the R2 group, 14.56–14.69 (14.62 ± 0.06) cm^3 in the R3 group and 14.23–14.67 (14.35 ± 0.19) cm^3 in the R4 group. The volume of the static image was 14.32–14.42 (14.37 ± 0.03) cm^3. The variance was largest in the R1 group, and a multi-group analysis of variance showed a significant difference ($P = 0.009$, Fig. 4a).

The percentage of overlap among the six images was 58.17% in the R1 group, 79.97% in the R2 group, 91.98%

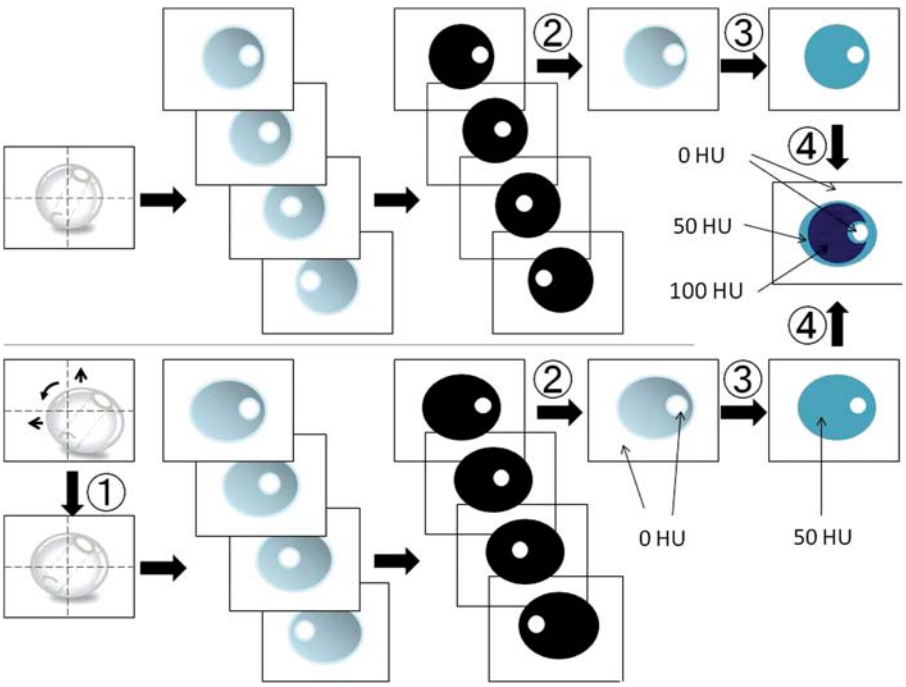

Fig. 3. Scheme of image analysis. [1] The image is shifted to the position where overlapping volume of the object yields the maximum value along the three horizontal and three rotational axes. CT image: second row from the left. Bitmap image obtained from the threshold: third row from the left. [2] Bitmap image is subtracted from the original CT data. HU outside of the bitmap turns to 0: second row from the right). [3] Any pixel data inside the image is changed to constant value (50 HU). [4] Fusion image represents overlapping volume in 100 HU, only one image volume in 50 HU and no image exists in 0 HU (right). In this study, six series of images were fused in the same way.

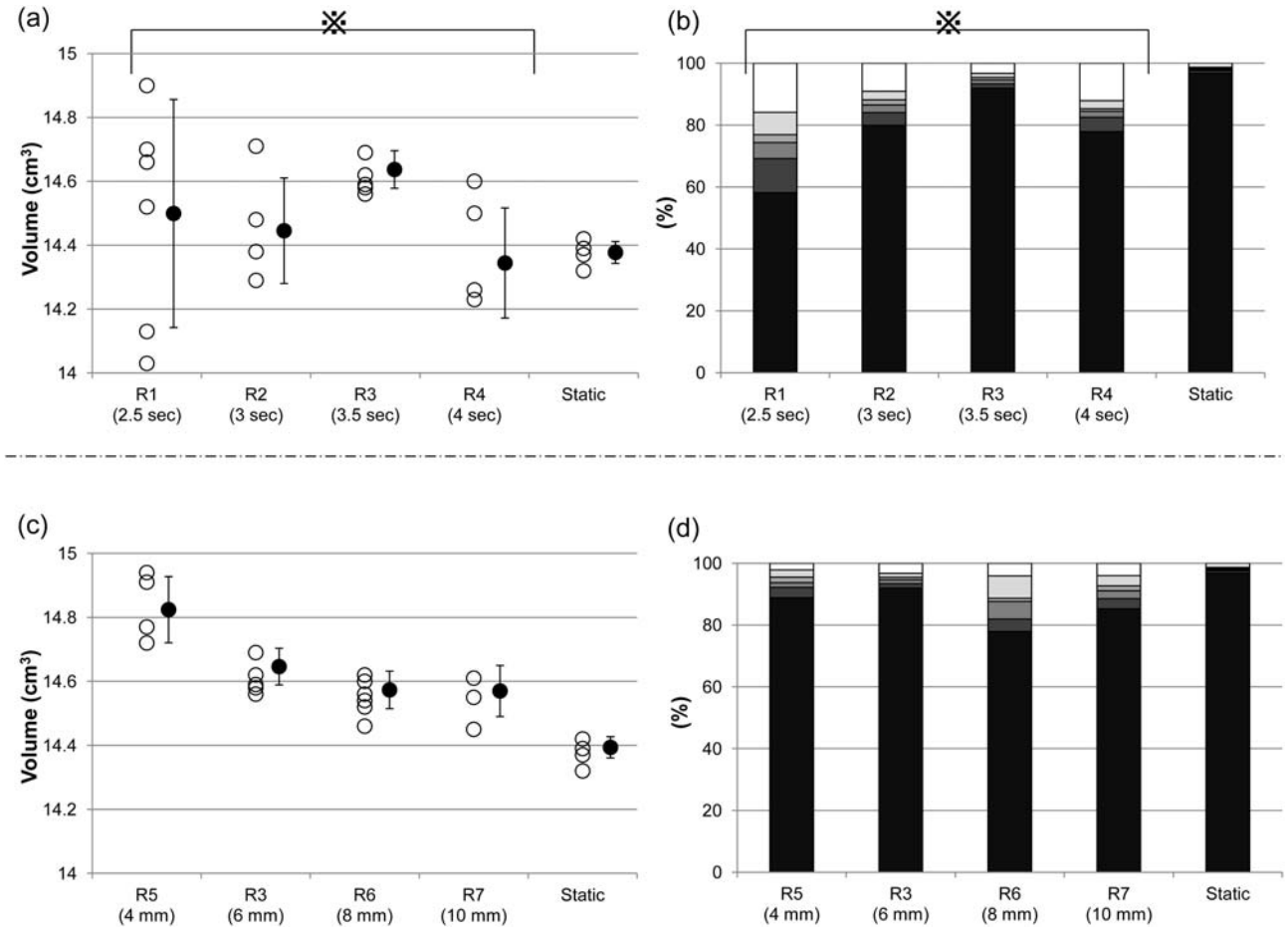

Fig. 4. Regular respiratory rhythms. Upper: Volume (**a**) and shape (**b**) variability in the cycle change study. Lower: Volume (**c**) and shape (**d**) variability in the amplitude change study. (a, c) Mean value and standard deviation are placed on the right. Large standard deviation represents large variability. (b, d) Each bar is divided into six columns according to the number of consistent images ((black column) on the bottom: all six object images are consistent, (white column) on the top: only one object image is present, without any other consistency). Small percentage of black column represents large variability. The static acquisition data is shown on the right as a reference. Volume (a): The volume variance shows a significant difference ($P = 0.009$). Shape (b): The shape variance shows a significant difference ($P = 0.002$). No significant change was observed in the volume (c) and shape (d) variability: ※ $P < 0.05$.

in the R3 group and 77.88% in the R4 group. The percentage of overlap among the six images was 96.8% in the static group. The percentage of overlap among the six images was smallest in the R1 group, and the chi-squared test showed a significant difference ($P = 0.002$, Fig. 4b).

Amplitude changes: R5 (4 mm), R3 (6 mm), R6 (8 mm) and R7 (10 mm).

The volume of the object was 14.72–14.94 (14.80 ± 0.10) cm^3 in the R5 group, 14.56–14.69 (14.62 ± 0.06) cm^3 in the R3 group, 14.46–14.62 (14.55 ± 0.06) cm^3 in the R6 group and 14.45–14.61 (14.55 ± 0.08) cm^3 in the R7 group. No significant difference was observed ($P = 0.523$, Fig. 4c).

The percentage of overlap among the six images was 88.79% in the R5 group, 91.98% in the R3 group, 77.85% in the R6 group and 85.24% in the R7 group. Although the R3 and R5 groups tended to have a higher percentage of overlap among the six images than the R6 and R7 groups, no significant difference was observed ($P = 0.52$, Fig. 4d).

Irregular respiratory rhythm study

Cycle changes: IR1 (3.5 + 2.5 s), IR2 (3.5 + 3 s), R3 (3.5 s) and IR3 (3.5 + 4 s).

The volume of the object was 14.91–15.42 (15.07 ± 0.19) cm^3 in the IR1 group, 14.93–15.48 (15.15 ± 0.24) cm^3 in the IR2 group, 14.56–14.69 (14.62 ± 0.06) cm^3 in the R3 group and 14.97–15.52 (15.32 ± 0.23) cm^3 in the IR3 group. The IR1, IR2 and IR3 groups tended to show a larger variance than the R3 group. A multi-group analysis of variance showed a significant difference ($P = 0.047$, Fig. 5a).

The percentage of overlap among the six images was 35.26% in the IR1 group, 90.41% in the IR2 group, 91.98% in the R3 group and 80.27% in the IR3 group. The

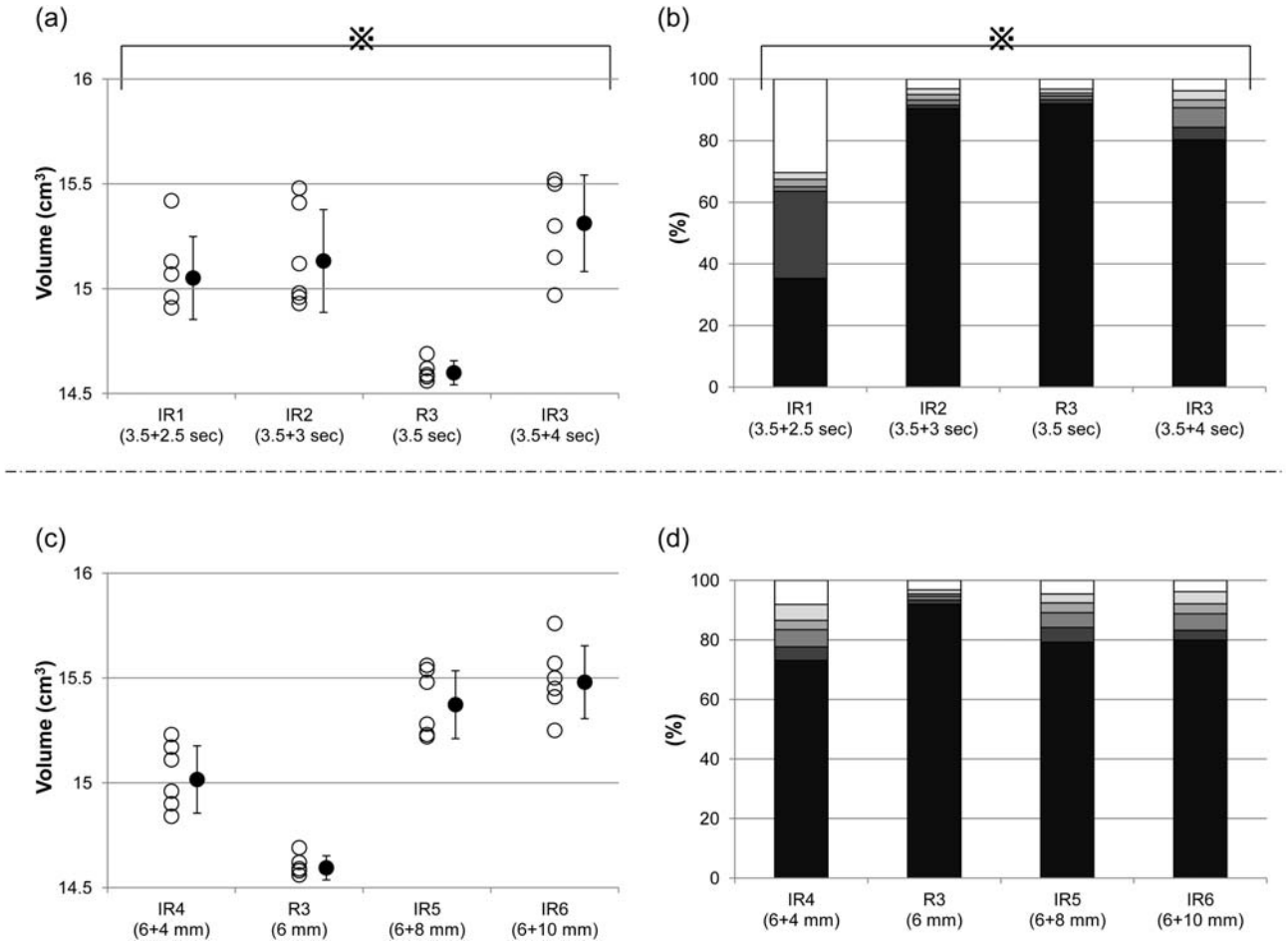

Fig. 5. Irregular respiratory rhythms. Upper: Volume (**a**) and shape (**b**) variability in the cycle change study. The regular respiratory data (R3: 3.5 s) is used as a substitute for 3.5 + 3.5 s. Lower: Volume (**c**) and shape (**d**) variability in the amplitude change study. Volume (a): The volume variance shows a significant difference ($P = 0.047$). Shape (b): The shape variance shows a significant difference ($P = 2.41 \times 10^{-24}$). No significant change was observed in the volume (c) and shape (d) variability. ※: $P < 0.05$

percentage of overlap among the six images was smallest in the IR1 group, and the chi-squared test showed a significant difference ($P = 2.41 \times 10^{-24}$, Fig. 5b).

Amplitude change: IR4 (6 + 4 mm), R3 (6 mm), IR5 (6 + 8 mm) and IR6 (6 + 10 mm).

The volume of the object was 14.84–15.23 (15.04 ± 0.16) cm^3 in the IR4 group, 14.56–14.69 (14.62 ± 0.06) cm^3 in the R3 group, 15.22–15.56 (15.39 ± 0.16) cm^3 in the IR5 group and 15.25–15.76 (15.49 ± 0.17) cm^3 in the IR6 group. Although the IR4, IR5 and IR6 groups tended to show a larger variance than the R3 group, no significant difference was observed ($P = 0.16$, Fig. 5c).

The percentage of overlap among the six images was 73.07% in the IR4 group, 91.98% in the R3 group, 79.19% in the IR5 group and 79.92% in the IR6 group. Although the IR4, IR5 and IR6 groups tended to have a lower percentage of overlap than the R3 group, no significant difference was observed ($P = 0.47$, Fig. 5d).

Figure 6 shows the image variability for regular and irregular respiratory cycle changes.

DISCUSSION

Any CT image has a risk of reduced image quality because of motion artifacts. Respiratory-gated data acquisition is frequently used for radiotherapy, and data acquisition at the end of exhalation is regarded to approximate stable imaging [8–10]. Past studies of image reproducibility have mainly focused on dislocation [6, 7, 16, 17], and image quality has seldom been investigated. However, a reduction in image reproducibility as a result of image quality loss is inevitable. Such reductions are greater for irregular CT beam exposure as a result of respiratory dysfunction or baseline drifting during the examination. Figure 6 clearly shows the difference between static and respiratory-gated images: the low-density area around the object was rectangular and

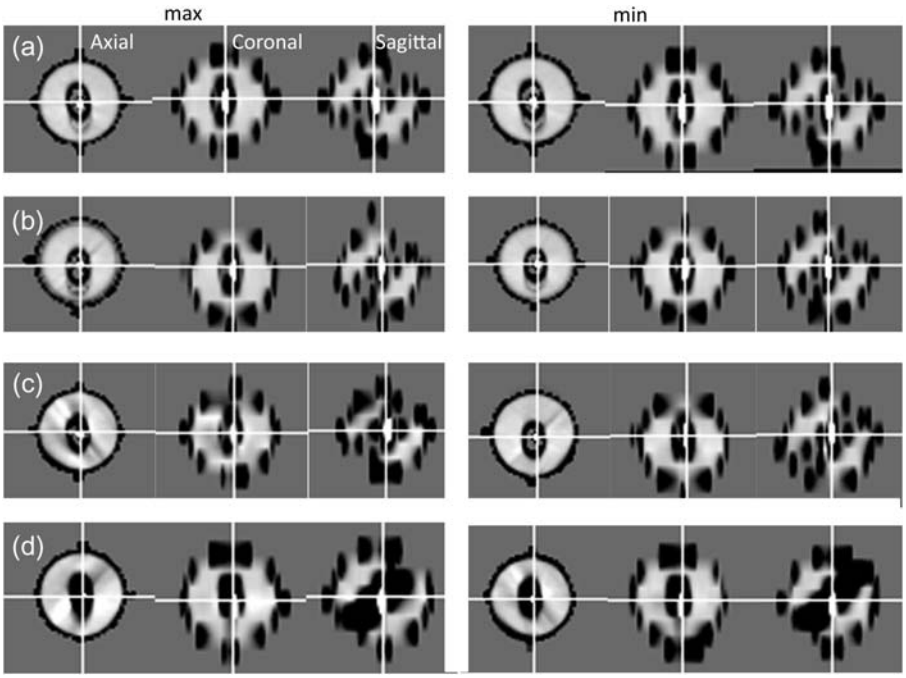

Fig. 6. CT Images of the object. (**a**) Static image group. (**b**) R3 (3.5 s) group. (**c**) R1 (2.5 s) group. (**d**) IR1 (3.5 + 2.5 s) group. The left series shows the maximum volume and the right series shows the minimum volume of the object image within the group. Each series contains an axial, coronal and sagittal image from the left. The cross lines pass through the metallic marker at the center.

quite similar among the static image group, whereas a portion of the low-density area around the object was deformed into a triangle and the difference in the distribution was clearer in the R3 group than in the static image group.

The scan speed [18,19], object volume [20] and scan phase [21–23] reportedly influence the reproducibility of moving objects in CT studies. However, to our knowledge, a basic investigation looking at respiratory rhythm and image reproducibility has not been fully performed. Our method has the advantage that many respiratory motion patterns can be reproduced using the phantom, the movement of which is similar to that of a human. The objectivity of this method is another advantage, as volume calculations can be performed using an auto-segmentation method without any manual processing.

As shown in the results, the volume and shape variability of the object changed markedly with cycle changes. The change was most prominent in the R1 group in the regular respiratory rhythm study and the IR1 group in the irregular respiratory rhythm study, both of which contained a 2.5-s cycle. For example, the volume of the object in the R1 group showed a 6% difference between the maximum and minimum volumes. The penetrated hole inside the object was indistinguishable on sagittal images, and the shape and distribution of the low-density area around the object exhibited a larger difference in the R1 group than in the R3 group. Moreover, the hole was hardly ever indistinguishable from the low-density area, and the shape of the low-density area was quite different from the axial and sagittal images in the IR1 group. Thus, a fast respiratory cycle may reduce image reproducibility not only independently, but also through an irregularly mixed appearance. On the other hand, the volume and shape variability of the object did not differ markedly with amplitude changes in the regular respiratory rhythms. The variability in the irregular amplitude change groups tended to be larger than that in the R3 group, which was regarded as the base rhythm; however, the variance was not as severe as the cycle change.

Lewis *et al.* reported that splitting artifacts occurred in situations where the scanning speed was greater than the maximum tumor velocity, and the measured tumor length could be shorter or longer than the true tumor length by a factor of up to the tumor velocity/translational scan velocity in their theoretical study of a four-dimensional CT (4DCT) model [18]. It is difficult to compare their 4DCT study and our respiratory-gated CT study. However, in the respiratory-gated system, as the translational scan velocity was a constant value (0), the image reproducibility should theoretically be mainly influenced by the tumor velocity. As the tumor velocity increases, the respiratory cycle would be shortened; consequently, their results may be consistent with our findings.

The CT beam exposure was performed for 1 s after the respiratory waveform dropped below the threshold (25% for

our system). Theoretically, the object should have moved from +3.0 mm to +5.52 mm rebounding through +6.0 mm in the R1 group, from +3.0 mm to +5.94 mm rebounding through +6.0 mm in the R2 group, and from +3.0 mm to +6.0 mm in the R3 and R4 groups in the cycle change study. In the amplitude change study, the object should have moved from +2.0 mm to +4.0 mm in the R5 group, +3.0 mm to +6.0 mm in the R3 group, +4.0 mm to +8.0 mm in the R6 group and +5.0 mm to +10.0 mm in the R7 group. In reality, because the beam exposure shifts with the decay time by a maximum of 0.25 s, the object movement should a little shift to the rebounding side than theoretical calculation. It is notable that the R3 group showed a higher reproducibility than any other group in the cycle change study. We consider that the object in the R3 group stays around the peak (+6.0 mm) during a longer period without moving upwards or downwards so much as the objects in the other groups. Thus, a cycle of 3.5 s may be the most suitable for this system.

The 2.5-s cycle could be criticized as being too fast for patients. Part of the reason we selected this short cycle is to make clear the trend of reproducibility of image along the cycle or amplitude change using a wide range. We previously measured the beam cycle of 25 patients with lung tumors, during 25 proton beam exposures [24]. Because correct measurement of the respiratory cycle was difficult for the patients with irregular respiratory patterns, we measured the cycle of the beam that is delivered when the respiratory waveform drops below the threshold as a surrogate. The beam cycle was mean 4.1, median 2.6 s. We consider the 2.5-s cycle of to be within the limits of reality.

This phantom can produce similar respiratory motion to humans in the point of coincident movement of the objects inside the lung field along with any respiratory motion of the chest wall and diaphragm. The results of this study give us a point to notice in respiratory-gated radiotherapy. Changes in the respiratory cycle of the patient reduces the reproducibility of image quality in respiratory-gated CT. Patients with irregular respiratory cycle have a particular risk of inadequate target delineation in planning CT. Education of patients with regard to achieving a stable and suitable respiratory rhythm or program improvements to correct inadequate respiratory motions could increase the reliability of CT imaging. However, patients' respiratory motion is much more complicated, especially due to the baseline shift. Further study is necessary to investigate this issue in detail.

CONCLUSION

Respiratory cycle changes reduced the reproducibility of image quality in a study using phantom model and respiratory-gated CT. The respiratory cycle should be carefully evaluated regardless of whether it has been well adapted with treatment planning.

FUNDING

This research is (partly) supported by the 'Funding Program for World-Leading Innovative R&D on Science and Technology (FIRST Program)', initiated by the Council for Science and Technology Policy (CSTP).

REFERENCES

1. Pan T, Sun X, Luo D *et al*. Improvement of the cine-CT based 4D-CT imaging. *Med Phys* 2007;**34**:4499–503.
2. Leng S, Zambelli J, Tolakanahalli R *et al*. Streaking artifacts reduction in four-dimensional cone-beam computed tomography. *Med Phys* 2008;**35**:4649–59.
3. Rietzel E, Chen GT. Improving retrospective sorting of 4D computed tomography data. *Med Phys* 2006;**33**:377–9.
4. Ohara K, Okumura T, Akisada M *et al*. Irradiation synchronized with respiration gate. *Int J Radiat Oncol Biol Phys* 1989;**17**:853–7.
5. Coolens C, Webb S, Shirato H *et al*. A margin model to account for respiration-induced tumour motion and its variability. *Phys Med Biol* 2008;**53**:4317–30.
6. Starkschall G, Balter P, Britton K *et al*. Interfractional reproducibility of lung tumor location using various methods of respiratory motion mitigation. *Int J Radiat Oncol Biol Phys* 2011;**79**:596–601.
7. Langner UW, Keall PJ. Accuracy in the localization of thoracic and abdominal tumors using respiratory displacement, velocity, and phase. *Med Phys* 2009;**36**:386–93.
8. Wu WC, Chan CL, Wong YW *et al*. A study on the influence of breathing phases in intensity-modulated radiotherapy of lung tumours using four-dimensional CT. *Br J Radiol* 2010;**83**:252–6.
9. Seppenwoolde Y, Shirato H, Kitamura K *et al*. Precise and real-time measurement of 3D tumor motion in lung due to breathing and heartbeat, measured during radiotherapy. *Int J Radiat Oncol Biol Phys* 2002;**53**:822–34.
10. Balter JM, Lam KL, McGinn CJ *et al*. Improvement of CT-based treatment-planning models of abdominal targets using static exhale imaging. *Int J Radiat Oncol Biol Phys* 1998;**41**:939–43.
11. Brady SL, Brown WE, Clift CG *et al*. Investigation into the feasibility of using PRESAGE/optical-CT dosimetry for the verification of gating treatments. *Phys Med Biol* 2010;**55**:2187–201.
12. Fukumitsu N, Sugahara S, Nakayama H *et al*. A prospective study of hypofractionated proton beam therapy for patients with hepatocellular carcinoma. *Int J Radiat Oncol Biol Phys* 2009;**74**:831–6.
13. Fukumitsu N, Hashimoto T, Okumura T *et al*. Investigation of the Geometric Accuracy of Proton Beam Irradiation in the Liver. *Int J Radiat Oncol Biol Phys* 2012;**82**:826–33.
14. Mizumoto M, Sugahara S, Okumura T *et al*. Hyperfractionated concomitant boost proton beam therapy for esophageal carcinoma. *Int J Radiat Oncol Biol Phys* 2011;**81**: e601–6.

15. Maes F, Collignon A, Vandermeulen D *et al*. Multimodality image registration by maximization of mutual information. *IEEE Trans Med Imaging* 1997;**16**:187–98.
16. van Sornsen de Koste JR, Cuijpers JP, de Geest FG *et al*. Verifying 4D gated radiotherapy using time-integrated electronic portal imaging: a phantom and clinical study. *Radiat Oncol* 2007;**2**:32.
17. Plathow C, Zimmermann H, Fink C *et al*. Influence of different breathing maneuvers on internal and external organ motion: use of fiducial markers in dynamic MRI. *Int J Radiat Oncol Biol Phys* 2005;**62**:238–45.
18. Lewis JH, Jiang SB. A theoretical model for respiratory motion artifacts in free-breathing CT scans. *Phys Med Biol* 2009;**54**:745–55.
19. Chen GT, Kung JH, Beaudette KP. Artifacts in computed tomography scanning of moving objects. *Semin Radiat Oncol* 2004;**14**:19–26.
20. Mutaf YD, Antolak JA, Brinkmann DH. The impact of temporal inaccuracies on 4DCT image quality. *Med Phys* 2007;**34**:1615–22.
21. Abdelnour AF, Nehmeh SA, Pan T *et al*. Phase and amplitude binning for 4D-CT imaging. *Phys Med Biol* 2007;**52**:3515–29.
22. Guckenberger M, Weininger M, Wilbert J *et al*. Influence of retrospective sorting on image quality in respiratory correlated computed tomography. *Radiother Oncol* 2007;**85**:223–31.
23. Rosen B, Starkschall G, Britton K *et al*. Utility of four-dimensional computed tomography for analysis of intrafractional and interfractional variation in lung volumes. *Int J Radiat Oncol Biol Phys* 2008;**72**:288–94.
24. Fukumitsu N, Oshiro Y, Hashimoto T *et al*. Verification of beam delivery using fibrosis after proton beam irradiation to the lung tumor. *Lung Cancer* 2012;**77**:83–6.